Excited-state Aromaticity Reversals in Möbius Annulenes

Peter B. Karadakov*,†, Make Di† and David L. Cooper‡

†Department of Chemistry, University of York, Heslington, York, YO10 5DD, U.K.

‡Department of Chemistry, University of Liverpool, Liverpool L69 7ZD, U.K.

Abstract

It is suggested that Möbius annulenes follow a rule similar to Baird's rule such that the $4n$ and $4n+2$ criteria for Möbius electronic ground state aromaticity and antiaromaticity are reversed in the lowest triplet and first singlet excited electronic states. Support comes from an investigation of aromaticity in the ground (S_0), lowest triplet (T_1) and first singlet excited (S_1) electronic states of the Möbius-aromatic cyclononatetraenyl cation, $C_9H_9^+$, using isotropic magnetic shielding isosurfaces calculated with state-optimized complete-active-space self-consistent field wave functions constructed from gauge-including atomic orbitals. Examination of these isosurfaces demonstrates that whereas the S_0 state of $C_9H_9^+$ is aromatic, the T_1 and S_1 states are antiaromatic.

1 Introduction

The idea of excited-state aromaticity reversals can be traced back to the Möbius-Hückel treatment of the transition states of pericyclic reactions, as was introduced by Dewar[1] and Zimmermann.[2] According to Dougherty's succinct summary,[3] thermal pericyclic reactions involving $4n+2$ electrons prefer Hückel transition states, whereas those involving $4n$ electrons prefer Möbius (anti-Hückel) transition states; these rules are reversed for photochemical reactions. A more detailed analysis carried out by Baird[4] led to the formulation of Baird's rule, which states that Hückel's $4n+2$ and $4n$ criteria for electronic ground state (S_0) aromaticity in cyclic conjugated hydrocarbons are switched in the lowest triplet state (T_1): Rings with $4n$ π electrons become aromatic while those with $4n+2$ π electrons end up as antiaromatic. Similar changes in aromaticity have been shown to take place in the lowest singlet excited state (S_1).[5–10] Excited-state aromaticity reversals in molecules with Hückel aromatic or antiaromatic electronic ground states have been attracting considerable theoretical and experimental interest.[11–15] Understanding this type of molecular behavior can help in the design of molecular photoswitches[15,16] and molecular motors,[17–19] and explain experimental evidence for photochemical reactions such as excited-state intramolecular proton transfers.[20,21] Theoretical studies suggest that excited-state aromaticity reversals are not limited to cyclic conjugated hydrocarbons but can also occur in inorganic rings, such as disulfur dinitride (S_2N_2);[22] S_0-T_1 aromaticity reversals have been predicted for several all-metal systems.[23]

Although less common than their Hückel counterparts, Möbius annulenes, which were conceived by Heilbronner[24] by re-arranging the overlapping 2p atomic orbitals (AOs) in an annulene ring along a Möbius strip, continue to serve as an important conceptual model. A detailed overview of pre-2005 research on Möbius aromaticity and delocalization can be found in Rzepa's review;[25] a pivotal moment in that period was the first synthesis of a Möbius aromatic hydrocarbon by Herges and co-workers in 2003.[26] More recent research includes establishing Möbius orbital topology in acyclic systems, such as linear

cumulenes,[27] and the synthesis of a Möbius tris((ethynyl)[5]helicene) macrocycle using alkyne metathesis.[28] Heilbronner's ideas about the electronic structure of Möbius annulenes have been confirmed in considerable detail using spin-coupled generalized valence bond (SCGVB) and complete-active-space self-consistent field (CASSCF) calculations.[29]

As mentioned above, it is well-known that Hückel's $4n + 2$ and $4n$ aromaticity rule is reversed for Möbius annulenes and that the aromatic cycles become those with $4n$ electrons, while those with $4n + 2$ electrons are antiaromatic. This is shown very clearly in Zimmerman's adaptation[2,30,31] of the familiar Frost-Musulin diagrams[32] to Möbius annulenes. In general, orbital arrays exhibiting Hückel or Möbius aromaticity involve even and odd numbers of phase changes (sign inversions), respectively.[31] Thus, it is natural to ask whether there is an analogue of Baird's rule for cyclic conjugated hydrocarbons with Möbius topology or, in other words, should it be expected that ground-state aromatic ($4n$) and antiaromatic ($4n + 2$) Möbius rings would experience aromaticity reversals in their lowest triplet states, becoming antiaromatic and aromatic, respectively? Would similar aromaticity reversals be observed in the lowest singlet excited states of such systems? Using resonance energies obtained from simple Hückel molecular orbital (HMO) theory, Aihara predicted[33] that any Hückel or Möbius annulene in its lowest excited state will have an aromaticity opposite to that in the ground state. While Aihara's approach is equivalent to, but easier to grasp, than preceding work based on perturbation molecular orbital (PMO) theory,[3,4] it remains subject to the oversimplifications inherent to HMO theory which cannot distinguish between singlet and triplet open-shell states and assumes that the lowest excited state arises entirely through a HOMO→LUMO orbital excitation. Rzepa and co-workers[34] discussed Möbius systems with $4n + 2$ electrons which become aromatic in their lowest triplet states. Using experimental measurements and density functional theory (DFT) calculations, Kim, Osuka and co-workers[35] showed that a singly-twisted [36]octaphyrin which is Möbius-aromatic in its S_0 state becomes antiaromatic in T_1.

Computationally, the T_1 state of any molecule is much easier to access than the S_1 state. A single-determinant spin-unrestricted Hartree-Fock (UHF) or Kohn-Sham UDFT calculation can provide a reasonable, albeit spin-contaminated, approximation to T_1, whereas the description of S_1 always requires a multideterminant wave function. This explains why most of the existing theoretical studies of excited state aromaticity reversals target the T_1 state although, from an experimental viewpoint, S_1 aromaticity reversals are more interesting, given that such reversals can be utilized to design molecules with phototuneable behaviour and explain excited-state reaction mechanisms.

In this paper we examine excited state aromaticity reversals in a Möbius ring using state-specific CASSCF wave functions which allow accurate descriptions, on an equal footing, of the S_0, T_1 and S_1 states. While benzene and square cyclobutadiene furnish realistic simple examples of ground-state Hückel aromatic and antiaromatic molecules, similarly realistic and simple examples of ground-state Möbius aromatic and antiaromatic molecules are more difficult to find. The smallest ground-state Möbius aromatic ring system known to date is the monocyclic cyclononatetraenyl cation, $C_9H_9^+$, which was shown by Mauksch *et al.*[36] to be Möbius-aromatic in its lowest-energy C_2 geometry. In a Heilbronner-style description (Figure 1), the $C_9H_9^+$ ring involves eight π electrons and nine carbon 2p AOs; accordingly, the SCGVB and CASSCF studies of the ground electronic state of this system were carried out assuming an "8 in 9" active space.[29]

Here we study aromaticity and bonding in the ground (S_0), first singlet excited (S_1) and lowest triplet (T_1) electronic states of $C_9H_9^+$ by analyzing the changes for each electronic state in the off-nucleus

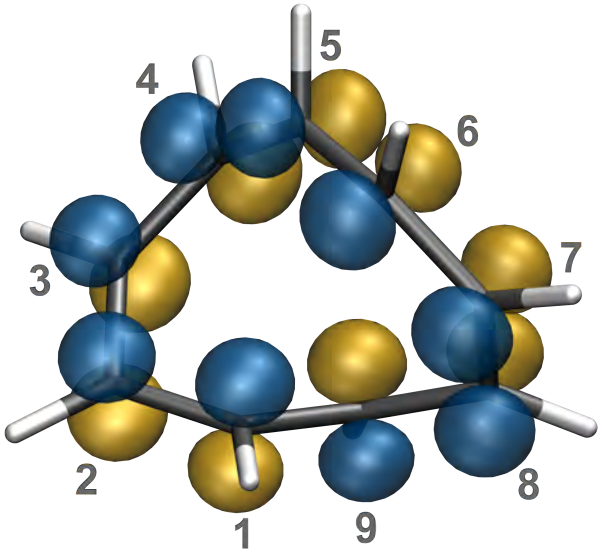

Figure 1: Heilbronner-style description of the ground electronic state of $C_9H_9^+$ obtained using Foster-Boys localized CASSCF(8,9)/aug-cc-pVTZ active space orbitals[29] which at isovalues of ± 0.2 closely resemble carbon 2p orbitals. The orbital phase change is between positions 1 and 9.

isotropic magnetic shielding, $\sigma_{\rm iso}(\mathbf{r}) = \frac{1}{3}[\sigma_{xx}(\mathbf{r}) + \sigma_{yy}(\mathbf{r}) + \sigma_{zz}(\mathbf{r})]$, in the space surrounding the molecule. While a popular aromaticity criterion, the single-point NICS(0), which is a type of nucleus-independent chemical shift and is defined as the value of $-\sigma_{\rm iso}$ at the center of the ring,[37] has already been applied to ground-state $C_9H_9^+$,[36,38] $\sigma_{\rm iso}(\mathbf{r})$ isosurfaces provide somewhat more detailed and, arguably, more reliable information about aromaticity and its effect on chemical bonding.[9,22,39] The large volume of data that is required to represent the off-nucleus magnetic isotropic shielding as a function of position addresses some potential deficiencies of single-point NICS, such as arbitrariness in the choice of locations at which such quantities are calculated (NICS can exhibit strong positional dependence and, in certain situations, standard choices can be inappropriate[40,41]) and the argument that a single number might not be sufficient to characterize all aspects of aromatic behavior, as is illustrated by the observation that different ring current maps can produce nearly indistinguishable single-point NICS values.[42,43]

2 Computational Procedure

Most of the calculations on $C_9H_9^+$ reported in this paper were carried out at the C_2 geometry of the $1\,^1$A electronic ground state optimized at the MP2(FC)/aug-cc-pVDZ level of theory.[29] The $\sigma_{\rm iso}(\mathbf{r})$ calculations for the low-lying electronic states of $C_9H_9^+$ utilized state-optimized CASSCF-GIAO wave functions (CASSCF with gauge-including atomic orbitals) in an "8 in 9" active space analogous to that adopted in ref. 29, defined within the standard 6-311+G(d) basis set. All CASSCF(8,9)-GIAO calculations were performed by means of the MCSCF-GIAO (multiconfigurational SCF with GIAOs) methodology[44,45] that is implemented in the Dalton program package.[46]

Given that we use the same ground-state geometry for all three electronic states of $C_9H_9^+$, the two excited electronic states correspond to vertical excitations. Following previous work on NICS[6,7,9,47] and ring currents[48] in triplet systems, the CASSCF-GIAO isotropic shieldings in the lowest triplet electronic state of $C_9H_9^+$ reported in this paper include only those contributions arising from the perturbation to

the wave function. With this choice, the values reported for a triplet state can be compared directly with those for singlet states. A more rigorous treatment would need to take into account the large terms associated with the interaction between the electronic spin angular momentum and the magnetic field.[49,50]

The grid of points used in the construction of $\sigma_{\rm iso}(\mathbf{r})$ isosurfaces for the S_0, T_1 and S_1 electronic states of $C_9H_9^+$ is regular with a spacing of 0.05 Å. It consists of 141 × 181 × 141 points and takes the shape of a 7 × 9 × 7 Å rectangular box with center and vertical coordinate axis (z) along the C_2 symmetry axis. In order to reduce computational effort, the $\sigma_{\rm iso}(\mathbf{r})$ values for each electronic state were calculated only for grid locations with nonnegative coordinates along one of the horizontal coordinate axes and they were then replicated by symmetry. For visualization purposes, all $\sigma_{\rm iso}(\mathbf{r})$ values obtained for the electronic states of $C_9H_9^+$ were assembled into GAUSSIAN cube files.[51]

Geometry optimizations and harmonic frequency calculations for the D_{9h} geometry and a related C_s geometry of triplet $C_9H_9^+$ were carried out at the UB3LYP-D3BJ/cc-pVTZ level (UB3LYP with Grimme's D3 empirical corrections and Becke-Johnson damping); for these calculations, and for a UB3LYP-GIAO/6-311+G(d) NICS calculation at the D_{9h} geometry, use was made of GAUSSIAN16.[52]

3 Results and Discussion

The energies of the state-optimized CASSCF(8,9)/6-311+G(d) wave functions for the S_0, T_1 and S_1 states of $C_9H_9^+$ are shown in Table 1 together with the corresponding S_0 to T_1 and S_0 to S_1 vertical excitation energies, NICS(0) values and isotropic magnetic susceptibilities, $\chi_{\rm iso} = \frac{1}{3}(\chi_{xx} + \chi_{yy} + \chi_{zz})$. For comparison, we show also vertical excitation energies, NICS(0) and $\chi_{\rm iso}$ values for the S_0, T_1 and S_1 states of benzene, calculated at the CASSCF(6,6)/6-311++G(2d,2p) level and taken from ref. 6. The NICS(0) indices for $C_9H_9^+$ were evaluated at the geometric center of the nine carbon atoms. The current ground electronic state NICS(0) of –14.07 ppm is close to the value of –13.4 ppm that was obtained by Mauksch *et al.*[36] at the RHF/6-31+G(d)//B3LYP/6-311+G(d,p) level. Those authors were surprised to find out that $C_9H_9^+$ has a ground electronic state NICS(0) lower than that of benzene. This is confirmed by the higher-level computational data in Table 1. The NICS(0) values appear to suggest that $C_9H_9^+$ in its ground electronic state is more aromatic than benzene, and this seems to be reinforced by comparing the ground electronic state $\chi_{\rm iso}$ values for the two molecules. However, the higher shielding at the center of $C_9H_9^+$ can be explained in a different way: The twisted shape of this cation brings shielded areas surrounding carbon-carbon bonds (see below) closer together than in benzene, increasing shielding at the center; the more negative isotropic magnetic susceptibility of $C_9H_9^+$ can thus be a consequence of its lower symmetry.

The large positive NICS(0) values in the T_1 and S_1 states of $C_9H_9^+$ indicate that these two states are antiaromatic, even more so than are the corresponding states of benzene. The difference between the levels of aromaticity of the T_1 and S_1 states of $C_9H_9^+$ is significantly larger than that between T_1 and S_1 in benzene, but in both cases the more antiaromatic state is S_1. These conclusions are supported by the changes in $\chi_{\rm iso}$ between different electronic states; the magnitudes of the T_1 and S_1 $\chi_{\rm iso}$ values in $C_9H_9^+$ are much larger than those in benzene, which can again be attributed to the lower symmetry of $C_9H_9^+$.

Other, arguably more accurate, NICS indices such as NICS(1), which is the value of $-\sigma_{\rm iso}$ at 1 Å above the center of the ring,[53,54] and NICS$(0)_{zz}$ and NICS$(1)_{zz}$, which are the values of $-\sigma_{zz}$ at the ring center[55,56] and at 1 Å above it,[57] respectively, cannot be applied to $C_9H_9^+$ because of the completely

Table 1: Total energies (E_h), vertical excitation energies ΔE (eV), NICS(0) values (ppm) and isotropic magnetic susceptibilities χ_{iso} (ppm cm^3 mol^{-1}) of the S_0, T_1 and S_1 electronic states of $C_9H_9^+$ calculated using CASSCF(8,9)-GIAO/6-311+G(d) wave functions at the MP2(FC)/aug-cc-pVDZ ground electronic state geometry; CASSCF(6,6)-GIAO/6-311++G(2d,2p) ΔE, NICS(0) and χ_{iso} values for the S_0, T_1 and S_1 electronic states of benzene[6] (units as for $C_9H_9^+$).

$C_9H_9^+$					Benzene			
State	Total Energy	ΔE	NICS(0)	χ_{iso}	State	ΔE	NICS(0)	χ_{iso}
S_0 ($1\,^1A$)	–345.863 899	0.00	–14.07	–81.05	S_0 ($1\,^1A_{1g}$)	0.00	–8.17	–59.33
T_1 ($1\,^3A$)	–345.741 337	2.56	42.23	35.48	T_1 ($1\,^3B_{1u}$)	3.86	39.63	–6.16
S_1 ($2\,^1A$)	–345.841 151	3.34	71.55	94.48	S_1 ($1\,^1B_{2u}$)	4.96	45.81	2.43

non-planar C_2 ground electronic state geometry. This even precludes fitting of a plane to the coordinates of the ring atoms, an approach which can be used for NICS(1)-style calculations on non-planar rings with small deviations from planarity.[58,59]

The variations in isotropic shielding around the S_0, T_1 and S_1 electronic states of $C_9H_9^+$ are illustrated in Figure 2. The isovalues of $\sigma_{iso}(\mathbf{r}) = \pm 16$ ppm and the orientations of the "side" and "top" views were chosen so as to show reasonable levels of detail; other orientations and isosurfaces for other isovalues can be examined using the GAUSSIAN cube files with isotropic shielding values for each of the three electronic states that are provided in the Supporting Information.

In the S_0 electronic ground state of $C_9H_9^+$, the uniform positive shielding enveloping all carbon-carbon bonds forms a twisted doughnut-like shape; shielding increases on the inside of the $\sigma_{iso}(\mathbf{r}) = 16$ ppm isosurface reaching up to between 38.3 and 42.0 ppm close to the midpoints of carbon-carbon bonds; there are no phase changes like that between orbitals 1 and 9 in Figure 1. This picture is similar to the shielding around benzene in its ground electronic state[9,39] and indicates strong bonding interactions and aromatic stability, although not up to benzene levels, as the carbon–carbon bonds in S_0 $C_9H_9^+$ are less shielded than are those in S_0 benzene, where $\sigma_{iso}(\mathbf{r})$ reaches 45.1 ppm at the midpoint of each carbon-carbon bond.[9] The small separation between the twists in the $\sigma_{iso}(\mathbf{r}) = 16$ ppm isosurface for S_0 $C_9H_9^+$ explains the large magnitude of the corresponding NICS(0) value; this observation shows that NICS(0) values should not be used to compare the relative aromaticities of the ground electronic states of $C_9H_9^+$ and benzene.

The isotropic shielding isosurfaces for the T_1 and S_1 electronic states of $C_9H_9^+$ are markedly different from those for the electronic ground state. The T_1 and S_1 electronic states of $C_9H_9^+$ are both dominated by sizable deshielded regions occupying most of the shape formed by the nine carbon atoms and extending well beyond this shape along the two directions not restricted by the molecular framework. The deshielded regions in the T_1 and S_1 electronic states of $C_9H_9^+$ (Figure 2) are larger in size and more irregular in shape than are the deshielded regions observed in the ground electronic state of square cyclobutadiene and in the T_1 and S_1 electronic states of benzene, where the presence of such deshielded regions has been shown to be the main factor weakening bonding interactions and causing antiaromatic destabilization.[9] The effect on bonding of the deshielded regions in each of the T_1 and S_1 electronic states of $C_9H_9^+$ is very similar to that observed in other antiaromatic electronic states:[9,22,39] The sizes

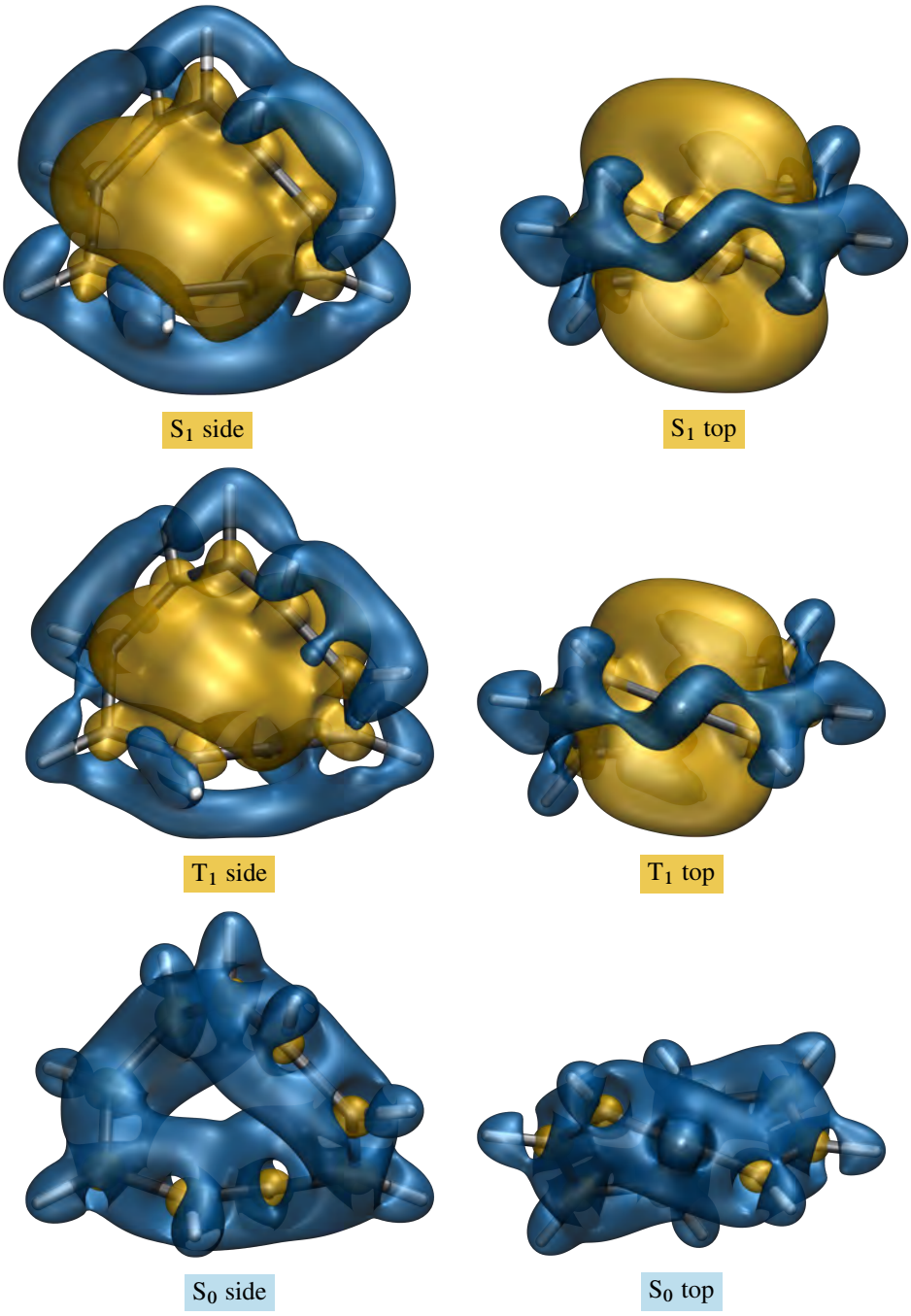

Figure 2: "Side" and "top" views of the isotropic shielding isosurfaces at $\sigma_{\mathrm{iso}}(\mathbf{r}) = \pm 16$ ppm for the S_0, T_1 and S_1 electronic states of $C_9H_9^+$ obtained using state-optimized CASSCF(8,9)-GIAO/6-311+G(d) wave functions (positive isovalue in blue).

of the shielded regions associated with individual C–C bonds are reduced considerably, to the point of disruption, and displaced outside the ring, away from the carbon-carbon bond directions. Examination of the isotropic shielding isosurfaces for the T_1 and S_1 electronic states of $C_9H_9^+$ does not provide a straightforward indication as to which of them is more antiaromatic: The central deshielded region is larger in S_1, but the shielded "band" around the molecule in this state is also thicker so that, on balance, T_1 and S_1 should exhibit similar levels of antiaromaticity in spite of the differences in NICS(0) and χ_{iso} values (Table 1). If allowed to relax after vertical excitation from S_0, both T_1 and S_1 can be expected to

assume less antiaromatic geometries.

While detailed analyses of the potential energy surfaces for the T_1 and S_1 electronic states of $C_9H_9^+$ fall outside the scope of this investigation, it should be noted that each of these potential energy surfaces could be anticipated to include an aromatic planar geometry of D_{9h} symmetry. To investigate this possibility for the T_1 state, we optimized the D_{9h} geometry of triplet $C_9H_9^+$ at the UB3LYP-D3BJ/cc-pVTZ level; this was followed by a harmonic frequency calculation. It turned out that, at this geometry (a regular nonagon with carbon-carbon and carbon-hydrogen bond lengths of 1.3996 Å and 1.0837 Å, respectively), triplet $C_9H_9^+$ has a doubly-degenerate imaginary frequency of $77.2i$ cm^{-1}. Relaxation of the D_{9h} geometry along one of the normal modes associated with this imaginary frequency, followed by re-optimization at the same level, produced a non-planar local minimum of C_s symmetry, corresponding to "folding" of the D_{9h} geometry along one of the C_2' symmetry axes. This result is not entirely unexpected, because the next annulene ring, [10]annulene, a Hückel $4n+2$ conjugated system which should be aromatic in its ground state, is well-known to have several local minimum conformers of similar energies, none of which is planar.[60,61] Similarly, the potential energy surfaces for the T_1 and S_1 electronic states of $C_9H_9^+$ can be expected to include various local mimima, the theoretical studies of which may become of interest when and if more experimental information about these states becomes available. The UB3LYP-GIAO/6-311+G(d) NICS(0) and NICS(1) values at the UB3LYP-D3BJ/cc-pVTZ optimized D_{9h} geometry of triplet $C_9H_9^+$ were obtained as -10.46 ppm and -10.43 ppm, respectively, and suggest benzene-like aromaticity which, however, proves insufficient to overcome the angle strain and prevent distortion to a geometry of lower symmetry.

The carbon nuclei in the ground electronic state of $C_9H_9^+$ are surrounded by small ovoid deshielded regions inside which the $\sigma_{iso}(\mathbf{r})$ values are negative (Figure 2). In the antiaromatic T_1 and S_1 states these ovoid deshielded regions around carbons merge with the larger deshielded region in the center of the molecule. Similar deshielded "halos" around sp^2 and sp hybridized carbons and other sp^2 hybridized first main row atoms have been observed previously in conjugated rings[9,39,62,63] as well as in open-chain conjugated molecules such as ethene, ethyne and *s-trans*-1,3-butadiene.[64] The occurrence of such "halos" has been attributed to a specific type of π electron behavior, characteristic of some sp^2 and sp hybridized first main row atoms, and that is different from traditional ring currents.[9] The observation of these "halos" in $C_9H_9^+$ confirms that the carbon atoms are close to sp^2 hybridized, which is in line with the Heilbronner-style description of this system (Figure 1) as well as the extensive shielding of the carbon-carbon bonds in the ground electronic state (Figure 2).

Analysis of the magnetic properties of ground, lowest triplet and first singlet excited electronic states of the smallest ground-state Möbius aromatic ring system known to date, the monocyclic cyclononatetraenyl cation, $C_9H_9^+$, shows that on vertical electronic excitation this cation exhibits aromaticity reversals similar to those in ground-state Hückel aromatic rings which are generally referred to as "Baird's rule". These results strongly suggest an excited-state aromaticity reversal rule for Möbius annulenes according to which, on vertical excitation to the lowest triplet or to the first singlet excited electronic state, those with $4n$ π electrons become antiaromatic whereas those with $4n+2$ π electrons could become aromatic.

Associated Content

Supporting Information

The Supporting Information is available free of charge at http://pubs.acs.org.

Optimized S_0 and T_1 geometries of $C_9H_9^+$ including NICS locations. Zip archive of GAUSSIAN cube files containing all of the $\sigma_{iso}(\mathbf{r})$ values used to construct the isotropic shieding isosurfaces for the S_0, T_1, and S_1 states of $C_9H_9^+$ reported in this work.

AUTHOR INFORMATION

Corresponding Author

*E-mail: peter.karadakov@york.ac.uk

ORCID

Peter B. Karadakov: https://orcid.org/0000-0002-2673-6804

David L. Cooper: https://orcid.org/0000-0003-0639-0794

Notes

The authors declare no competing financial interest.

REFERENCES

(1) Dewar, M. J. S. A Molecular Orbital Theory of Organic Chemistry—VIII: Aromaticity and Electrocyclic Reactions. *Tetrahedron* **1966**, *22*, 75–92.

(2) Zimmerman, H. E. On Molecular Orbital Correlation Diagrams, the Occurrence of Möbius Systems in Cyclization Reactions, and Factors Controlling Ground- and Excited-State Reactions. I. *J. Am. Chem. Soc.* **1966**, *88*, 1564–1565.

(3) Dougherty, R. C. A Perturbation Molecular Orbital Treatment of Photochemical Reactivity. The Nonconservation of Orbital Symmetry in Photochemical Pericyclic Reactions. *J. Am. Chem. Soc.* **1971**, *93*, 7187–7201.

(4) Baird, N. C. Quantum Organic Photochemistry. II. Resonance and Aromaticity in the Lowest $^3\pi\pi^*$ State of Cyclic Hydrocarbons. *J. Am. Chem. Soc.* **1972**, *94*, 4941–4948.

(5) Kataoka, M. J. Magnetic Susceptibility and Aromaticity in the Excited States of Benzene. *Chem. Res.* **2004**, 573–574.

(6) Karadakov, P. B. Ground- and Excited-State Aromaticity and Antiaromaticity in Benzene and Cyclobutadiene. *J. Phys. Chem. A* **2008**, *112*, 7303–7309.

(7) Karadakov, P. B. Aromaticity and Antiaromaticity in the Low-Lying Electronic States of Cyclooctatetraene. *J. Phys. Chem. A* **2008**, *112*, 12707–12713.

(8) Feixas, F.; Vandenbussche, J.;Bultinck, P; Matitoe, E.; Solà, M. Electron Delocalization and Aromaticity in Low-lying Excited States of Archetypal Organic Compounds. *Phys. Chem. Chem. Phys.* **2011**, *13*, 20690–20703.

(9) Karadakov, P. B.; Hearnshaw, P.; Horner, K. E. Magnetic Shielding, Aromaticity, Antiaromaticity, and Bonding in the Low-Lying Electronic States of Benzene and Cyclobutadiene. *J. Org. Chem.* **2015**, *81*, 11346–11352.

(10) Ponec, R.; Cooper, D. L.; Karadakov, P. B. Are Multicentre Bond Indices and Related Quantities Reliable Predictors of Excited-State Aromaticity? *Molecules* **2020**, *25*, 4791(1–14).

(11) Rosenberg, M.; Dahlstrand, C.; Kilså, K.; Ottosson, H. Excited State Aromaticity and Antiaromaticity: Opportunities for Photophysical and Photochemical Rationalizations. *Chem. Rev.* **2014**, *114*, 5379–5425.

(12) Papadakis, R.; Ottosson, H. The Excited State Antiaromatic Benzene Ring: A Molecular Mr Hyde? *Chem. Soc. Rev.* **2015**, *44*, 6472–6493.

(13) Ottosson, H.; Borbas, K. E. A Light-Switched Yin and Yang Pair. *Nature Chem.* **2015**, *7*, 373–375.

(14) Sung, Y. M.; Yoon, M.-C.; Lim, J. M.; Rath, H.; Naoda, K.; Osuka, A.; Kim, D. *Nature Chem.* **2015**, *7*, 418–422.

(15) Durbeej, B.; Wang, J.; Oruganti, B. Molecular Photoswitching Aided by Excited-State Aromaticity. *ChemPlusChem* **2018**, *83*, 958–967.

(16) Skov, A. B.; Ree, N.; Gertsen, A. S.; Chabera, P.; Uhlig, J.; Lissau, J. S.; Nucci, L.; Pullerits, T.; Mikkelsen, K. V.; Brøndsted Nielsen, M. et al. Excited-State Topology Modifications of the Dihydroazulene Photoswitch Through Aromaticity. *ChemPhotoChem* **2019**, *3*, 619–629.

(17) Oruganti, B.; Wang, J.; Durbeej, B. Excited-State Aromaticity Improves Molecular Motors: A Computational Analysis. *Org. Lett.* **2017**, *19*, 4818—4821.

(18) Wang, J.; Oruganti, B.; Durbeej, B., A Straightforward Route to Aromatic Excited States in Molecular Motors that Improves Photochemical Efficiency. *ChemPhotoChem* **2019**, *3*, 450–460.

(19) Oruganti, B.; Pál Kalapos, P.; Bhargav, V.; London, G.; Durbeej, B. Photoinduced Changes in Aromaticity Facilitate Electrocyclization of Dithienylbenzene Switches. *J. Am. Chem. Soc.* **2020**, *142*, 13941–13953.

(20) Lampkin, B. J.; Nguyen, Y. H.; Karadakov, P. B.; VanVeller, B. Demonstration of Baird's Rule Complementarity in the Singlet State with Implications for Excited-State Intramolecular Proton Transfer. *Phys. Chem. Chem. Phys.* **2019**, *21*, 11608–11614.

(21) Karas, L. J.; Wu, C.-H.; Ottosson, H.; Wu, J. I. Electron-Driven Proton Transfer Relieves Excited-State Antiaromaticity in Photoexcited DNA Base Pairs. *Chem. Sci.* **2020**, *11*, 10071–10077.

(22) Karadakov, P. B.; Al-Yassiri, M. A. H.; Cooper, D. L. Magnetic Shielding, Aromaticity, Antiaromaticity and Bonding in the Low-Lying Electronic States of S_2N_2. *Chem. Eur. J.*, **2018**, *24*, 16791–16803.

(23) Chen, D.; Szczepanik, D. W.; Zhu, J.; Solà, M. All-metal Baird Aromaticity. *Chem. Commun.* **2020**, *56*, 12522–12525.

(24) Heilbronner, E. Hückel Molecular Orbitals of Möbius-type Conformations of Annulenes. *Tetrahedron Lett.* **1964**, *29*, 1923–1928.

(25) Rzepa, H. S. Möbius Aromaticity and Delocalization. *Chem. Rev.* **2005**, *105*, 3697–3715.

(26) Ajami, D.; Oeckler, O.; Simon, A.; Herges, R. Synthesis of a Möbius Aromatic Hydrocarbon. *Nature* **2003**, *426*, 819–821.

(27) Garner, M. H.; Hoffmann, R.; Rettrup, S.; Solomon, G. C. Coarctate and Möbius: The Helical Orbitals of Allene and Other Cumulenes. *ACS Cent. Sci.* **2018**, *4*, 688–700.

(28) Jiang, X.; Laffoon, S. D.; Chen, D.; Pérez-Estrada, S.; Danis, A. S.; Rodríguez-López, J.; Garcia-Garibay, M. A.; Zhu, J; Moore, J. S. Kinetic Control in the Synthesis of a Möbius Tris((ethynyl)[5]helicene) Macrocycle Using Alkyne Metathesis. *J. Am. Chem. Soc.* **2020**, *142*, 6493-–6498.

(29) Karadakov, P. B.; Cooper, D. L. Does the Electronic Structure of Möbius Annulenes Follow Heilbronner's Ideas? *ChemPhysChem*, **2018**, *19*, 3186–3190.

(30) Zimmerman, H. E. Molecular Orbital Correlation Diagrams, Möbius Systems, and Factors Controlling Ground- and Excited-State Reactions. II. *J. Am. Chem. Soc.* **1966**, *88*, 1566–1567.

(31) Zimmerman, H. E. The Möbius-Hückel Concept in Organic Chemistry. Application to Organic Molecules and Reactions. *Acc. Chem. Res.* **1971**, *4*, 272–280.

(32) Frost, A. A.; Musulin, B. A Mnemonic Device for Molecular Orbital Energies. *J. Chem. Phys.* **1953**, *21*, 572–573.

(33) Aihara, J. Aromaticity-Based Theory of Pericyclic Reactions. *Bull. Chem. Soc. Jpn.* **1978**, *51*, 1788–1792.

(34) Kastrup, C. J.; Oldfield, S. P.; Rzepa, H. S. The Aromaticity and Möbius Characteristics of Carbeno[8]heteroannulenes and Triplet State Annulenes. *Chem. Commun.* **2002**, 642–643.

(35) Hong, Y.; Oh, J.; Sung, Y. M.; Tanaka, Y.; Osuka, A.; Kim, D. The Extension of Baird's Rule to Twisted Heteroannulenes: Aromaticity Reversal of Singly and Doubly Twisted Molecular Systems in the Lowest Triplet State. *Angew. Chem. Int. Ed.* **2017**, *56*, 2932–2936.

(36) Mauksch, M.; Gogonea, V.; Jiao, H.; Schleyer, P. v. R. Monocyclic $C_9H_9^+$—A Heilbronner Möbius Aromatic System Revealed. *Angew. Chem. Int. Ed.* **1998**, *37*, 2395–2397.

(37) Schleyer, P. v. R.; Maerker, C.; Dransfeld, A.; Jiao, H.; van Eikema Hommes, N. J. R. Nucleus-Independent Chemical Shifts: A Simple and Efficient Aromaticity Probe. *J. Am. Chem. Soc.* **1996**, *118*, 6317–6318.

(38) Bucher, G.; Grimme, S.; Huenerbein, R.; Auer, A. A.; Mucke, E.; Köhler, F.; Siegwarth, J.; Herges, R. *Angew. Chem. Int. Ed.* **2009**, *48*, 9971–9974.

(39) Karadakov, P. B.; Horner, K. E. Magnetic Shielding in and around Benzene and Cyclobutadiene: A Source of Information about Aromaticity, Antiaromaticity and Chemical Bonding. *J. Phys. Chem. A* **2013**, *117*, 518–523.

(40) Foroutan-Nejad, C.; Shahbazian, S.; Feixas, F.; Rashidi-Ranjbar, P.; Solà, M. A Dissected Ring Current Model for Assessing Magnetic Aromaticity: A General Approach for Both Organic and Inorganic Rings *J. Comput. Chem.* **2011**, *32*, 2422–2431.

(41) Foroutan-Nejad, C. Is NICS a Reliable Aromaticity Index for Transition Metal Clusters? *Theor. Chem. Acc.* **2015**, *134:8*, 1–9.

(42) Fias, S.; Fowler, P. W.; Delgado, J. L.; Hahn, U.; Bultinck, P. Correlation of Delocalization Indices and Current-Density Maps in Polycyclic Aromatic Hydrocarbons. *Chem. Eur. J.* **2008**, *14*, 3093–3099.

(43) Van Damme, S.; Acke, G.; Havenith, R. W. A.; Bultinck, P. Can the Current Density Map Topology be Extracted from the Nucleus Independent Chemical Shifts? *Phys. Chem. Chem. Phys.* **2016**, *18*, 11746–11755.

(44) Ruud, K.; Helgaker, T.; Kobayashi, R.; Jørgensen, P.; Bak, K. L.; Jensen, H. J. A. Multiconfigurational Self-Consistent Field Calculations of Nuclear Shieldings Using London Atomic Orbitals. *J. Chem. Phys.* **1994**, *100*, 8178–8185.

(45) Ruud, K.; Helgaker, T.; Bak, K. L.; Jørgensen, P.; Olsen, J. Accurate Magnetizabilities of the Isoelectronic Series BeH^-, BH, and CH^+. The MCSCF-GIAO Approach. *Chem. Phys.* **1995**, *195*, 157–169.

(46) Aidas, K.; Angeli, C.; Bak, K. L.; Bakken, V.; Bast, R.; Boman, L.; Christiansen, O.; Cimiraglia, R.; Coriani, S.; Dahle, P. et al. *WIREs Comput. Mol. Sci.* **2014**, *4*, 269–284; *Dalton, a Molecular Electronic Structure Program, Release Dalton2018.1*, **2019**, see http://daltonprogram.org.

(47) Gogonea, V.; Schleyer, P. v. R.; Schreiner, P. R. Consequences of Triplet Aromaticity in $4n\pi$-Electron Annulenes: Calculation of Magnetic Shieldings for Open-Shell Species. *Angew. Chem. Int. Ed.*, **1998**, *37*, 1945–1948.

(48) Fowler, P. W.; Steiner, E.; Jenneskens, L. W. Ring-current Aromaticity in Triplet States of $4n$ π electron monocycles. *Chem. Phys. Lett.* **2003**, *371*, 719–723.

(49) Rinkevicius, Z.; Vaara, J.; Telyatnyk, L.; Vahtras, O. Calculations of Nuclear Magnetic Shielding in Paramagnetic Molecules. *J. Chem. Phys.* **2003**, *118*, 2550–2561.

(50) Vaara, J. Theory and Computation of Nuclear Magnetic Resonance Parameters. *Phys. Chem. Chem. Phys.* **2007**, *9*, 5399–5418.

(51) See http://www.gaussian.com/g_tech/g_ur/u_cubegen.htm.

(52) Frisch, M. J.; Trucks, G. W.; Schlegel, H. B.; Scuseria, G. E.; Robb, M. A.; Cheeseman, J. R.; Scalmani, G.; Barone, V.; Petersson, G. A.; Nakatsuji, H. et al. *Gaussian 16*, Revision A.03; Gaussian, Inc.: Wallingford CT, 2016.

(53) Schleyer, P. v. R.; Jiao, H.; van Eikema Hommes, N. J. R.; Malkin, V. G.; Malkina, O. L. An Evaluation of the Aromaticity of Inorganic Rings: Refined Evidence from Magnetic Properties. *J. Am. Chem. Soc.* **1997**, *119*, 12669–12670.

(54) Schleyer, P. v. R.; Manoharan, M.; Wang, Z. X.; Kiran, B.; Jiao, H.; Puchta, R.; van Eikema Hommes, N. J. R. Dissected Nucleus-Independent Chemical Shift Analysis of π-Aromaticity and Antiaromaticity. *Org. Lett.* **2001**, *3*, 2465–2468.

(55) Cernusak, I.; Fowler, P. W.; Steiner, E. Ring Currents in Six-Membered Heterocycles: The Diazaborinines $(CH)_2B_2N_2$. *Mol. Phys.* **2000**, *98*, 945–953.

(56) Steiner, E.; Fowler, P. W.; Jenneskens, L. W. Counter-Rotating Ring Currents in Coronene and Corannulene. *Angew. Chem. Int. Ed.* **2001**, *40*, 362–366.

(57) Fallah-Bagher-Shaidaei, H.; Wannere, C. S.; Corminboeuf, C.; Puchta, R.; Schleyer, P. v. R. Which NICS Aromaticity Index for Planar π Rings is Best? *Org. Lett.* **2006**, *8*, 863–866.

(58) Matito, E.; Poater, J.; Duran, M.; Solà, M. An Analysis of the Changes in Aromaticity and Planarity along the Reaction Path of the Simplest Diels–Alder Reaction. Exploring the Validity of Different Indicators of Aromaticity. *J. Mol. Struct. THEOCHEM* **2005**, *727*, 165–171.

(59) Dobrowolski, J. Cz.; Lipiński, P. F. J. On Splitting of the NICS(1) Magnetic Aromaticity Index. *RSC Adv.* **2016**, *6*, 23900–23904.

(60) King, R. A.; Crawford, T. D.; Stanton, J. F.; Schaefer III, H. F. Conformations of [10]Annulene: More Bad News for Density Functional Theory and Second-Order Perturbation Theory. *J. Am. Chem. Soc.* **1999**, *121*, 10788–10793.

(61) Dimitrova, M.; Sundholm, D. The Aromatic Character of [10]Annulenes and Dicupra[10]Annulenes from Current Density Calculations. *Phys.Chem.Chem.Phys.* **2018**, *20*, 1337–1346.

(62) Horner, K. E.; Karadakov, P. B. Chemical Bonding and Aromaticity in Furan, Pyrrole, and Thiophene: A Magnetic Shielding Study. *J. Org. Chem.* **2013**, *78*, 8037–8043.

(63) Horner, K. E.; Karadakov, P. B. Shielding in and around Oxazole, Imidazole, and Thiazole: How Does the Second Heteroatom Affect Aromaticity and Bonding? *J. Org. Chem.* **2015**, *80*, 7150–7157.

(64) Karadakov, P. B.; Horner, K. E. Exploring Chemical Bonds through Variations in Magnetic Shielding. *J. Chem. Theory Comput.* **2016**, *12*, 558–563.

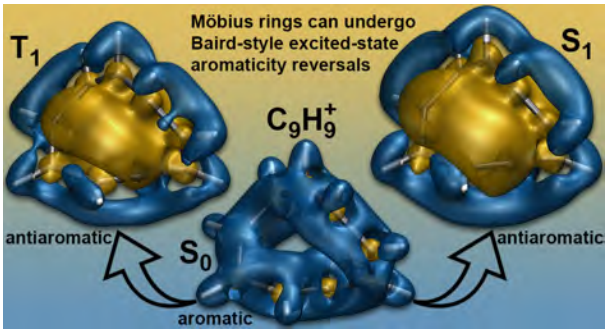

Table of Contents/Abstract Graphic

Supporting Information

Excited-state Aromaticity Reversals in Möbius Annulenes

Peter B. Karadakov*,†, Make Di† and David L. Cooper‡

†Department of Chemistry, University of York, Heslington, York, YO10 5DD, U.K.
‡Department of Chemistry, University of Liverpool, Liverpool L69 7ZD, U.K.

*E-mail: peter.karadakov@york.ac.uk

Gaussian Cube Files with Isotropic Shielding Values

A zip archive of GAUSSIAN cube files containing all of the $\sigma_{iso}(\mathbf{r})$ values used to construct the isotropic shielding isosurfaces for the S_0, T_1, and S_1 states of $C_9H_9^+$ reported in the current work is available as a separate download.

Optimized Geometries

All coordinates are in Å. All geometries, at which NICS calculations were carried out specify the respective positions as 'X' atoms.

C_2 geometry of the electronic ground state of $C_9H_9^+$ optimized at the MP2(FC)/aug-cc-pVDZ level of theory, taken from ref. 29.

```
C 0. 0. 1.645014194
C 0.4905022324 1.2427684773 1.1554414148
C -0.4905022324 -1.2427684773 1.1554414148
C 0.0100585215 2.0928052569 0.1040785875
C -0.0100585215 -2.0928052569 0.1040785875
C -0.8152087457 1.6410894083 -0.9354914584
C 0.8152087457 -1.6410894083 -0.9354914584
C -0.6569284614 0.2832859329 -1.251946014
C 0.6569284614 -0.2832859329 -1.251946014
H 0. 0. 2.7459418542
H 1.0699783805 1.7858874614 1.9137457041
H -1.0699783805 -1.7858874614 1.9137457041
H 0.12964425 3.1677255378 0.2859658405
H -0.12964425 -3.1677255378 0.2859658405
H -1.5936377795 2.2790433661 -1.3665504299
H 1.5936377795 -2.2790433661 -1.3665504299
H -1.490812806 -0.3325910524 -1.6109751404
H 1.490812806 0.3325910524 -1.6109751404
X 0.0 0.0 -0.023424527
```

D_{9h} saddle point geometry of the lowest triplet state of $C_9H_9^+$ optimized at the UB3LYP-D3BJ/cc-pVTZ level of theory.

```
C
C 1 cc
C 2 cc 1 140.
C 3 cc 2 140. 1 0. 0
C 4 cc 3 140. 2 0. 0
C 5 cc 4 140. 3 0. 0
C 6 cc 5 140. 4 0. 0
C 7 cc 6 140. 5 0. 0
C 8 cc 7 140. 6 0. 0
H 1 hc 2 110. 3 180. 0
H 2 hc 3 110. 4 180. 0
H 3 hc 4 110. 5 180. 0
H 4 hc 5 110. 6 180. 0
H 5 hc 6 110. 7 180. 0
H 6 hc 7 110. 8 180. 0
```

```
H 7 hc 8 110. 9 180. 0
H 8 hc 9 110. 1 180. 0
H 9 hc 1 110. 2 180. 0

cc=1.39958901
hc=1.08365777
```

The positions at which NICS(0) and NICS(1) were calculated in the standard center-of-mass orientation were

```
X 0.0 0.0 0.0
X 0.0 0.0 1.0
```

C_s local minimum geometry of the lowest triplet state of $C_9H_9^+$ optimized at the UB3LYP-D3BJ/cc-pVTZ level of theory.

```
C 0.0718558694 -1.2909878981 1.5234035555
C 0.4004437727 0. 1.9464013268
C 0.0718558694 1.2909878981 1.5234035555
C -0.3769156634 1.9195274884 0.3555945338
C -0.2050793841 1.7065178123 -1.0128332384
C 0.3080538876 0.6973246976 -1.8391144713
C 0.3080538876 -0.6973246976 -1.8391144713
C -0.2050793841 -1.7065178123 -1.0128332384
C -0.3769156634 -1.9195274884 0.3555945338
H 0.1491568035 -2.0006138161 2.3411315292
H 0.8235866713 0. 2.9440005358
H 0.1491568035 2.0006138161 2.3411315292
H -0.7758957922 2.9061177487 0.5610611211
H -0.4242085846 2.6039063935 -1.5820794464
H 0.6372975725 1.0960087597 -2.7923509975
H 0.6372975725 -1.0960087597 -2.7923509975
H -0.4242085846 -2.6039063935 -1.5820794464
H -0.7758957922 -2.9061177487 0.5610611211
```